IEEE Robotics and Automation Letters (RAL) paper presented at the
2020 IEEE/RSJ International Conference on Intelligent Robots and Systems (IROS)
October 25-29, 2020, Las Vegas, NV, USA (Virtual)

Milliscale Features Increase Friction of Soft Skin in Lubricated Contact

Monica S. Li, Dominic Melville, Ethan Chung and Hannah S. Stuart

***Abstract*— Real world environments, such as kitchens, present objects covered in viscous fluids: soap, oil, water, etc. Understanding and designing for slippery and submerged contact, where fluid lubrication is present, is a continuing challenge in the robotics community. Contact area, bending stiffness, and the presence of a viscous fluid affect friction. This work focuses on milliscale features (3 to 20 mm in size) of soft urethane skin on smooth, flat surfaces. We characterize the friction of soft skins, with varying size, and therefore bending stiffness, of cylindrical features, all with the same nominal contact area. In addition, a new method of frustrated total internal reflection with dye is introduced to visualize lubricated contact. We find that a small number of milliscale fingertip features maximizes friction force in the presence of lubrication, as compared both to un-patterned and many-featured skin designs. This holds true for a robotic gripper test, when pinching glass submerged in oil.**

I. INTRODUCTION

Dexterous robots assisting in real world applications must capably execute manual tasks in the presence of variable contact conditions [1]. This work focuses on the wet and submerged environments present in applications varying from home service robots to remote ocean exploration. For example, dish-washing robots are being developed for at-home operation [2] and commercial purposes [3]. Robotic hands must grip objects covered in water, soap, oil, biofilms, etc. (Fig. 1). Slippery contact conditions can make it difficult to grasp objects with strength and reliability, and grasping with higher normal forces is not always feasible. This is especially true when handling fragile items like glassware. Modification of contact conditions through careful skin design can combat this slippery challenge. As stated in [4], "like the performance of a sports car which is ultimately limited by the tires on its wheels, the performance of a robotic hand is limited by the skin on its fingers."

A. Soft robotic skin for frictional contact

Increasing friction through careful skin selection can aid in achieving force closure during robotic grasping [6]. Soft rubber is a popular skin option that distributes contact loads, reducing localized stress concentrations that could break fragile objects during grasping. Soft skin can also comply passively to an object's roughness and geometry, enabling interlocking between the surfaces. The details of geometry (i.e. number and shape of surface features) and material of soft skins contribute to their contact conditions. For example, in dry conditions, compliant cylindrical pads composed of a stiffer material result in higher friction [7]. One soft skin model describes how a set of discrete elastic cantilevers, where the stick-slip of each beam is modeled with Coulomb friction, can be combined to model friction of the system as a whole [8].

Fig. 1: Examples of manipulation with lubricated contact – a) The Robotiq gripper picks up a ceramic mug while using a set of soft fingerpads on extended fingertips. The latter of which prevents fluid exposure to electronics. b) Person washes dishes where water, soap and food residue make the pan slippery. Inset: Pressure distribution of a human fingertip that is wrinkly after prolonged exposure to wet conditions, cast in silicone rubber and pressed against the high-resolution tactile sensor developed for [5].

A number of works characterize how soft skin in dry contact conditions can be selected and controlled when applied to robotic manipulation. Grasp robustness is evaluated on a parallel-jaw gripper with silicone fingertips for a variety of surface features [9]. A friction-tunable soft finger pneumatically induces ridges to control friction properties [10]. An increase in pressure is modeled and observed to increase the height of the finger's ridges and friction forces. In [11], a geometric surface design can passively switch between high and low contact area depending on normal force; it can either firmly grasp or slide past surfaces for different tasks. Friction of compliant fingertips is intentionally decreased by

This work was supported by the University of California at Berkeley. The work of M. S. Li was supported by the NASA Space Technology Research Fellowship, under Grant 80NSSC19K1166 for sensitive end-effector design for spiny attachment onto frangible substrates in extreme underwater environments. The work of E. Chung was supported by the Rose Hills Summer Undergraduate Research Fellowship.

M. S. Li, D. Melville, E. Chung and H. S. Stuart are with Embodied Dexterity Group, Department of Mechanical Engineering, University of California at Berkeley, Berkeley, CA 94720 USA (email: monicasli@berkeley.edu; dominic.melville@berkeley.edu; ec2021@berkeley.edu; hstuart@berkeley.edu). *Corresponding author: Monica Li.*

introducing fluid onto a slitted surface in [12]. These works do not address increasing friction during lubricated contact.

Researchers have noted how the fingerpads of humans, and some primates, wrinkle after prolonged exposure to water, shown in the inset of Fig. 1. The debate regarding the evolutionary role of water-induced wrinkling, and whether it improves the mechanics of manipulation in wet and submerged environments, is still ongoing [13]–[15]. A leading argument asserts that the tread-like features at the fingertips can enhance contact by reducing lubrication, similar to how treads reduce slipping on automobile tires and shoe soles, as in [16,17]. However, a physical explanation that details the fluid lubrication effects with skin surface features, such as treads, still remains ambiguous. Recently, Mizushima, et al. [18] compared textured surfaces in dry and lubricated conditions to find that the size and shape of surface features affect friction. They focus on features 1 - 4 mm in size and found that slits perpendicular to the loading direction exhibit the highest friction coefficient when wet, among their tested geometries. The current study expands upon these findings to include large (>4 mm) cylindrical features. We also test whether trends for viscous squeeze flow translate to prehensile pinching in a real robotic hand.

B. Comparison to other contact technologies

Frictional soft skin is only one of many robotic contact solutions. For wet conditions, researchers are designing micropatterned surfaces that employ *capillary effect* for adhesion, enabling tasks like picking up a contact lens without squeezing [19]. Capillary effect can produce adhesion on wet surfaces [20] but is not applicable for grasping completely submerged objects as it relies on surface tension. *Gecko inspired adhesives* enable robots to resist large-scale shear forces on clean, dry surfaces [21,22]. While surface functionalization can allow synthetic gecko adhesives to perform in wet conditions [23], it has not been applied to robotic manipulation. On rough surfaces, *microspines* are highly effective for applying tangential loads with a multifinger hand [24]. Spines have been applied effectively underwater via the JPL Nautilus Gripper that attaches onto rocks in the deep ocean [25] and a gripper composed of sets of blunted teeth for grasping hard corals [26]. However, interlocking with spines is not suitable for grasping smooth, flat, hard surfaces or when a surface should not be marred. *Suction* can enhance grasping, especially in submerged environments, and a constant suction flow at the fingertip increases grasp region of a hand [27]. This modality requires additional pumps and tubing to be installed on the robotic device. Contact technologies may also be combined. For example, a bio-inspired attachment mechanism utilizes both a suction seal and spines to grip onto smooth and rough surfaces underwater, resisting large normal and tangential forces [28].

We focus on passive, soft skin due to its mechanical simplicity, easy fabrication and integration, as well as its versatility in a wide number of applications.

C. Overview

Models for friction, bending stiffness and viscous fluid squeeze flow are presented in Section II. Section III details the fabrication and experimental set-up used in testing frictional behaviors. A new method of visualizing lubricated contact area using frustrated total internal reflection is introduced. In Section IV, we find that an un-patterned soft skin has low friction in submerged conditions. Otherwise, friction force increases with bending stiffness of the surface features, a trend that holds true for dry and submerged trials. Lubricated friction force is therefore maximized at intermediate feature patterns. Section V discusses how the models for bending stiffness and lubrication support our experimental results. Section VI highlights that milliscale skin features can enhance robotic grasping and describes future work for contact area imaging.

II. Friction Models and Fluid Effects on Contact

Models of dry friction, surface feature bending stiffness and viscous squeeze flow between two disks are detailed for comparison with experimental results in Section IV.

A. Contact models for dry friction

The simplest friction model is Coulomb or Amonton's Law, which models friction force as proportional to normal force, related by a friction coefficient μ. Based on Hertzian elastic contact theory, friction force is proportional to the contact area between two surfaces; between a half-sphere and a flat plane, contact area is proportional to normal force to the two-thirds power [29]:

$$F_{fr} \propto R^2 \propto F_N^{2/3} \tag{1}$$

with tangential or friction force F_{fr}, radius of contact R, and normal force F_N. Surface interactions between rubber and rigid objects typically match the Hertzian friction model [30]. In actuality, friction is more nuanced. A power-scaling modification to Hertzian contact is used to more accurately model contact mechanics of soft robotic fingers, where contact radius is proportional to normal force to the 0-1/3 power [31]. This is an accurate model for elastic spherical contacts, but changes in skin geometry and the presence of a lubricating film can have significant effects on friction that are not captured. In Section IV-C, we test for a trend between contact area and friction, with cylindrical features in lubricated conditions.

B. Bending stiffness of cylindrical surface features

Previously, researchers found that pad stiffness can either increase or decrease friction in dry conditions, depending on contact geometry [32]. For the cylindrical pad in contact with a flat, rigid face, researchers observed an increase in friction with increasing stiffness [7]. For skin pads with constant nominal contact area and feature height, varying the number of features changes their bending stiffness. A cantilevered

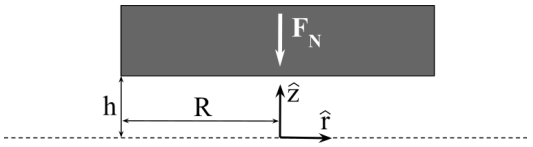

Fig. 2: Schematic diagram for the Stefan-Reynolds equation that describes two parallel disks symmetrically squeezing together, showing only the top disk and the dashed center-line (representing the glass plate in this simplified model). The disk moves down at speed $\dot{h}$ given squeeze force F_N, as fluid flows out of the gap with height h.

beam with circular cross-section has stiffness k and moment of inertia I

$$k = \frac{3EI}{L^3}, \quad I = \frac{\pi R^4}{4} \tag{2}$$

with modulus of elasticity E, length of beam L, and mathematical constant π. Assuming the superposition of stiffness for parallel features gives the total stiffness of a given skin pad, bending stiffness would decrease with the inverse of the number of features n. That is,

$$k_{tot} \propto n^{-1} \ . \tag{3}$$

In practice, when not all features are in contact with a surface, stiffness will be effectively lower. Furthermore, tangential forces deform flexible features, shifting contact to the edges. In the extreme case, flexible features bend so much that the cylinder walls are in contact with the surface. Bending stiffness estimated with Eqn. (2) is used when observing friction trends in Sec. IV-A.

C. Squeeze force of viscous fluid between two disks

The presence of a thin fluid film between end-effector and object can create slippery contact and result in grasp failure. For manipulation tasks in wet and submerged environments, dynamic fluid interactions must be taken into account. Derived in the Appendix and shown in the schematic diagram (Fig. 2), the Stefan-Reynolds equation describes fluid flow squeezing out of the gap between two parallel disks [33]. Assuming a Newtonian, incompressible fluid and the appropriate boundary conditions, the normal squeeze force to decrease the gap height, F_N, is

$$F_N = -\frac{3}{8}\frac{\pi\eta\dot{h}R^4}{h^3} \tag{4}$$

with fluid viscosity η, closing velocity $\dot{h}$, radius R, and gap height h. Keeping all else constant, the squeeze force is proportional to viscosity, and in air this squeeze force usually goes unnoticed. The dynamic viscosity of canola oil, η_{oil}=5x10^{-2} kg/m·s [34], is more than three orders of magnitude greater than that of air, η_{air}=2x10^{-5} kg/m·s. Water has a dynamic viscosity of η_{water}=8x10^{-3} kg/m·s. Increasing the radius of a disk exponentially increases force, indicating less force is required to squeeze smaller areas closer together. For a constant nominal contact area, contact consisting of many smaller circles rather than one large contact lowers total squeeze force required. Specifically, the squeeze force for all the contacts $F_{N,\,tot}$ is also proportional to the inverse of feature number:

$$F_{N,\,tot} \propto n^{-1} \ . \tag{5}$$

Typically, thicker lubrication layers result in lower friction [35]. We expect fluid lubrication effects to be most apparent in robotic hands with smooth, flat skin. Based on the analysis in Sections II-B and II-C, we expect a trade-off between stiffness and lubrication, which are both related to feature size.

III. Experimental Methods

This study tests soft skin pads with circular features of varying size and quantity with the same total nominal contact area. We use feature sizes up to 20 mm in diameter to fit on a humanoid robotic fingertip. The frictional behavior of skin pads is measured on dry glass and glass submerged in canola oil. Lubricated real contact area is imaged applying a modified frustrated total internal reflection technique.

A. Design and fabrication of soft skin pads

We designed soft skin pads to evaluate how surface feature size affects friction. Cylinders of varying size and quantity compose the surface features of the skin pads. Features fall within the same enclosed footprint and are circular to reduce asymmetry. (This is additionally addressed by changing orientation of the pads by 90^o between the experiments described in Sec. III-B and III-C.) Surface features of each skin pad have a combined area of 32.3 mm^2 (1/2 in^2), approximately the area of a United States penny. To evenly fit circular features into the same enclosed footprint, skin pads have 1, 3, 7, 13, 19, 31 and 55 features. Fabrication consists of casting urethane into negative molds, lasercut from acrylic. The size of the laser was accounted for to ensure constant nominal contact area across the different skins. The sets of skins were cast with urethane rubber of Shore A 30, 50, and 80 hardness (Smooth-On Vytaflex 30, 50 and Econ 80) with 100% modulus of 0.45, 1.48, 4.62 MPa, respectively. The bending stiffness of these contact pads ranges from 4.5 N/m for 55 Shore A 30 hardness features to 2600 N/m for the single 80A feature. All the features are 6.4 mm in height and are set on a 6.4 mm thick base, shown in Fig. 3.

B. Friction of soft skin on smooth glass

The friction of these skin pads is tested on glass submerged in canola oil and clean, dry glass (Fig. 4 left). A 200 g mass is fixed above the skin pad, providing a normal force of approximately 2 N. A Mark-10 Series 4 force gauge is used

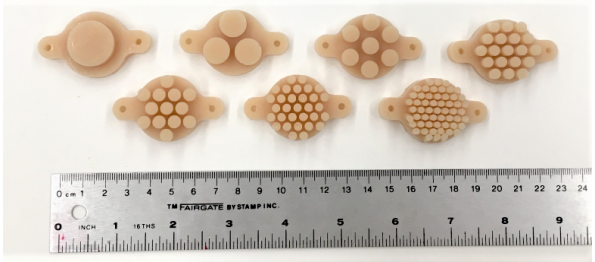

Fig. 3: Photograph of soft skins cast with Shore A 30 hardness urethane (100% modulus = 0.45 MPa). The total area of 32.3 mm^2 of each pad is divided into 1, 3, 7, 13, 19, 31 and 55 circular features. Both feature and base height are 6.4 mm.

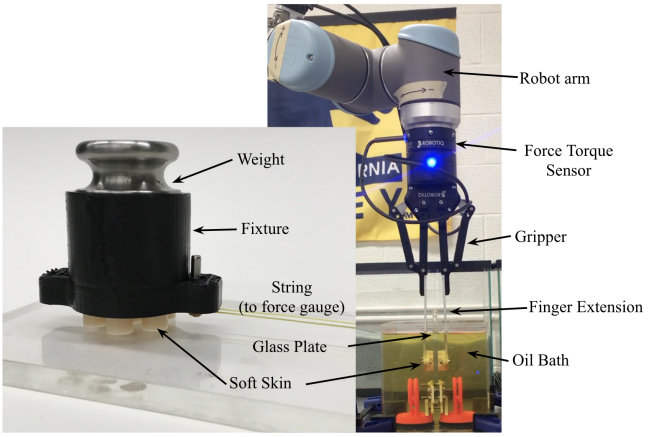

Fig. 4: Experimental setup. Left: single-axis pull experiments. A soft skin and weight are fixed to a 3D printed mount. With a string attached to a force gauge, the skin is dragged across smooth glass, dry or submerged in oil, and the force is recorded real-time. Right: robotic arm with soft skin attached on the fingertips. The skin pinches and pulls up on a glass plate submerged in oil, and pullout force is recorded.

to measure tangential forces as the weighted skin is dragged across a glass plate at approximately 10 cm/s via a tensioned string. Tangential force is recorded at 10 Hz averaged over one second for 10 trials. This measured force is divided by normal force for the kinetic friction coefficient. In this work we will refer to the *friction coefficient* of contact as the ratio of tangential to normal force, even though we acknowledge that it is only applicable to the specific testing conditions used, such as shearing rate.

C. Robotic pinching in a bath of oil

The internal squeezing force of a pinch grasp constrains contact surfaces differently than the constant normal force in the previous experiment. To verify translation of the results from weighted, single-axis experiments to robotics, the middle stiffness, 100% modulus = 1.48 MPa (Shore A 50 hardness), skin pads are also tested on a robotic gripper system. Skin pads are attached to extended fingertips of a 2-finger 140 Robotiq adaptive gripper for opposed pinching. The gripper is mounted on the UR10 robot arm from Universal Robots. The gripper pinches a glass plate in an oil bath and then moves upwards, dragging the skin pads across the glass with the positional uncertainty and drift of a real robotic system (Fig. 4 right). The Robotiq FT 300 Force Torque Sensor is used to measure pullout force of the glass. The squeeze force is approximately 4 N for the hard pinch and a 2 N for the light pinch. We compare this to dry pinching; however, the shear grasping forces were so high on the glass plate that a wooden block was used instead to avoid damage or finger wear. The finger pads are mounted to the robotic grasper such that they are loaded in an orientation perpendicular to the experiment in Sec. III-B, to capture effects of contact feature orientation.

D. Contact imaging

An estimate of contact area is compared with measured friction force for dry and lubricated conditions. Real contact area between two surfaces often differs from apparent, or

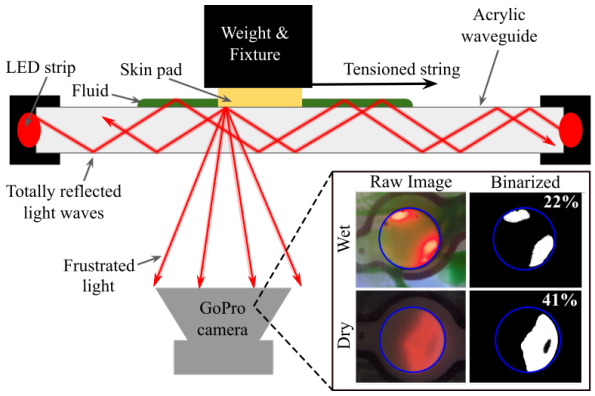

Fig. 5: Schematic diagram of frustrated TIR technique setup. Light waves that initially undergo total internal reflection are scattered or frustrated from the acrylic waveguide by contact of the skin pad. This light is detected by a camera underneath and is used to estimate contact area. In the lubricated case, a fluid is selected that transmits the light while the pigmented fluid partially absorbs light such that skin pad contact is illuminated and the fluid is not. Raw frusturated TIR images and post-processing to calculate percent of real contact area (inset) are shown for wet and dry conditions. Nominal contact area is outlined in blue.

nominal, contact area. Frustrated total internal reflection (TIR) is an optical technique used to measure real contact area [36]. LED lights with a red filter are wrapped around the edges of a 13 mm thick acrylic waveguide, as in Fig. 5. This technique relies on the difference in index of refraction between acrylic and air, 1.49 and 1.00 respectively, to achieve TIR.

When a surface comes into contact with one side of the waveguide, the red light scatters and is frustrated from the waveguide to the other side and recorded by a video camera (GoPro Hero4). In the lubricated case, a propylene glycol based dye (Americolor Candy Oil, green), refractive index similar to acrylic (1.43), covers the plate. We infer that the dye transmits light while maintaining TIR at the air interface. We chose a liquid with heavy pigment that absorbs transmitted light, thus enabling a measure of contact film thickness. Here, we assume a binary measure of contact based on color saturation and brightness of image. This measure is sensitive to post-processing and threshold selection. Characterizing the relationship between illumination, force and film thickness will be a part of future work. Even in dry conditions researchers have found increasing signal intensity with normal force [36].

The inset of Fig. 5 shows an example of the raw frustrated TIR image and contact area calculation of a single contact in wet and dry conditions. Images for dry contact were captured 0.1 sec before total slip and then matched with peak friction force. For the lubricated case, images and force measurements were taken midway through sliding. All images were collected using skin pads cast with Shore A 50 hardness urethane. A 100 g weight corresponding to 1 N of normal force was used for dry imaging because the heavier weight made tangential motion too difficult. Post-processing of images with a red color filter and binarization is used to calculate the percentage of real contact area compared to nominal contact area.

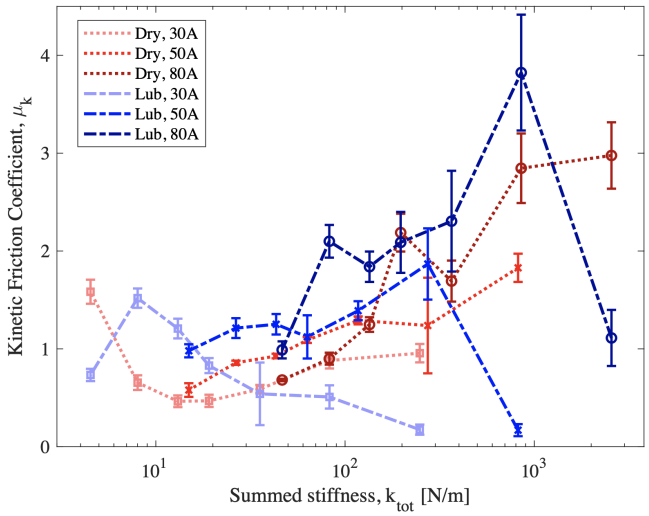

Fig. 6: Kinetic friction coefficient versus bending stiffness of the soft skin pads. The test specimen were molded from urethane with hardness of Shore 30A, 50A, 80A. Experimental results are shown for friction on glass for dry (red) and lubricated (i.e. submerged in oil, blue) contact conditions.

IV. Results

A. Skin friction: feature size and stiffness

The kinetic friction of all skin designs in this study are plotted against total skin stiffness in Fig. 6. Overall for the harder materials (Shore A 50 and 80 hardness), there is a positive correlation between summed stiffness and kinetic friction. Kinetic friction coefficient of submerged un-patterned skin is the exception. In the presence of a lubricating fluid, the un-patterned skin pad requires little force to move, i.e. it is very slippery. This is consistent with previous studies where a smooth fingerpad was compared with textures of 1 mm lengthscale [18]. For dry contact, the un-patterned skin pad exhibits the highest friction coefficient: between 1 and 3 for the skin materials tested. Differences between dry and submerged kinetic friction are less apparent in skins with multiple surface features. The softest skin (Shore A 30 hardness) demonstrates increasing kinetic friction at the lowest stiffness range. We infer that the softest and most flexible features deform significantly during the experiments, resulting in new contact effects such as contact with the side walls of the features.

B. Robotic gripper pinch test

The mean and standard deviation of 30 gripper pullout force trials using Shore A 50 hardness pads, normalized with squeeze force, are plotted over the duration of the robotic grasping trials, shown in Fig. 7 for three cases: a strong (a) and light (c) pinch on glass submerged in canola oil, and on a dry wooden block (d). The static and kinetic friction from Fig. 7 (a) are synthesized in Fig. 7 (b). In oily conditions, pullout force for un-patterned contact was initially unnoticeable and gradually increased as the skin pads slid across the plate. Skin pads with surface features had an initial peak pullout force then maintained relatively constant forces. Lower pullout forces are observed for pads with many surface features, matching trends observed in Fig. 6. Thus, the friction trends from controlled lab experiments translate

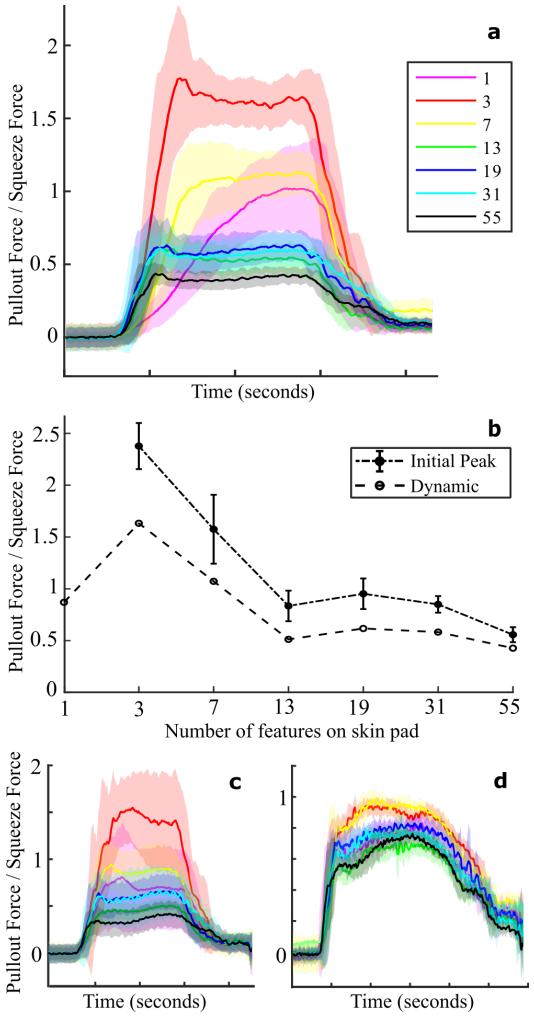

Fig. 7: Pullout force of the robotic gripper pinching, averaged across 30 trials. (a) shows a pinch and pull test on a glass plate submerged in canola oil, with a squeeze force of approximately 4 N. (b) summarizes data from (a) to display static and kinetic friction coefficient of the skin pads. Additional pullout forces for (c) a light grasp on oily glass and (d) dry wood show that the effect of skin features in submerged conditions does not translate to dry conditions.

to more realistic grasping. In addition, any effect due to feature orientation, by rotating the finger pad orientation, is not observed.

A light pinch grasp yields similar results as hard grasping. Note that, under grasp forces of approximately 4 N smaller features visibly deformed as the skin was dragged across the glass but this was not observed with 2 N grasping. On dry wood, we observed no significant difference in pullout force for different surface features.

C. Contact Area Imaging

Imaging using the frustrated TIR technique provides insight for contact interactions between deformable and rigid surfaces. Presented in Fig. 8, we observe that contact area is not a strong indicator of friction force, indicating that Hertzian contact theory may not prove useful for these conditions. Note that, as described in Sec. III-D, we are using an estimate of contact area specific to our sensor, so the results depend on this particular measurement method.

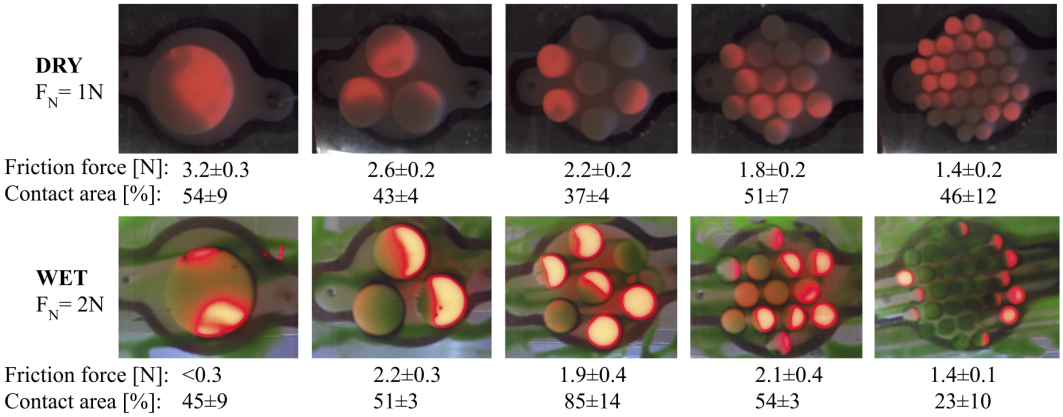

Fig. 8: Contact area images taken using frustrated TIR for skin pads with 1, 3, 7, 13, and 31 features in dry and wet conditions. Friction and percent of real to nominal contact area are listed (N=4). Skin pads of Shore A 50 hardness are dragged across acrylic with a 1 N normal force. For dry contact, peak friction force and area 0.1 sec prior to total slip are recorded. Force and area measurements are taken midway through sliding in the lubricated case. The skin pads have the same nominal contact area, but exhibit clear differences in contact geometry.

For dry contact, the soft skin does not slide. Rather, we observe a stick-slip behavior; sections of the pad are stuck to the surface while other sections are in motion, not in contact at all. The weight and fixture above the skin jiggle as portions of the skin surface undergo stick-slip. When a rigid sphere moves across rubber at a fixed displacement distance, rather than a fixed force, researchers observe waves of contact and detachment and conclude that no true sliding occurs [37], consistent with our observations.

Fluid lubrication enables the skin to move across the glass with a smoother sliding motion. Lubricated friction trends match with those found in the submerged tests, indicating that wet and submerged contact behave in similar ways in this study. Whether the two surfaces ever make real contact or are separated by a thin fluid film is unclear. Even if the surfaces make no real contact, shearing of the fluid in the gap produces a restraining force analogous to friction. In our observations, higher normal force increases real contact area as the features initially in contact comply, allowing contact of more features. When friction forces are especially high, we observe pronounced contact at the leading edge of the surface feature. We also note that the contact patches move around as the skin slides in the lubricated case; different surface features come into and out of contact with the plate. For the un-patterned pad, the contact patches move towards the trailing edge.

V. Discussion

This study supports the expectation that there is a trade-off between feature stiffness and lubrication effect, both related to feature size, in the design of fingertip skin that maximizes friction for the handling of submerged surfaces. For the specific patterns tested, the stiffest skin pad material with three discrete features (each approximately 12 mm in diameter) provides the highest friction in lubricated conditions. This is an atypical robotic finger pad pattern. Increasing friction in this manner can help to improve the ability of robot hands to perform force closure and reduce the chance of dropping slippery objects, as compared with completely smooth or highly-patterned skins. Other robotics works, such as in [4], have discussed how friction predictability proves desirable for the control of robotic devices, rather than simply maximizing peak friction ability. Ultimately, skin selection for dexterous manipulation is a multi-faceted problem.

VI. Conclusions

The design of milliscale features on the skin of robotic grippers can improve grasp security. Our results indicate that robots working in lubricated contact conditions may benefit from soft skin with a few surface features – as opposed to one or many – to achieve higher friction. Potential applications for this simple solution range from home assistance to remote exploration, when water and other lubricants are present.

A. Future work

A broadened scope of models and experiments can further establish the underlying mechanisms of slippery surfaces. Lubrication theory and the field of elastohydrodynamics, coupled with numerical modeling, may provide a more detailed physical explanation to observed behaviors. Testing a number of different skin surface properties, such as heights and geometries, will also produce new perspectives on parametric scaling properties. This work presents a frustrated TIR technique with pigmented fluid to measure contact area in both dry and lubricated conditions; decrypting the characteristics of this sensor via controlled distance, illumination and force experiments could yield new insights into fluid lubrication on soft structures and is a promising area for future investigation.

Appendix
Stefan-Reynolds equation derivation

The following shows the derivation of Eqn. (4) and (5) from Section II-C. We assume a Newtonian and incompressible fluid. Conservation of mass and momentum for a control volume between the two disks can be respectively expressed as $-\dot{h}\pi r^2 = 2\pi r \int_0^h v_r dz$ and $0 = -\frac{\partial p}{\partial r} + \eta \frac{\partial^2 v_r}{\partial z^2}$ with closing velocity $\dot{h}$, gap height h, radius r, and radial velocity v_r. The boundary conditions include no slip at the disk surface, maximum flow at the axial center, and atmospheric pressure (zero gauge pressure) outside the disks: $v_r(z =$

$\pm h) = 0$, $\frac{\partial v_r}{\partial z}(z = 0) = 0$, $p(r = R) = 0$. Integrating the momentum equation twice with respect to z and using boundary conditions to solve for constants, the radial velocity is $v_r = \frac{1}{2\eta}\frac{\partial p}{\partial r}\left(z^2 - h^2\right)$. Using this formulation for v_r in mass conservation and integrating over r, pressure at the disk surface is $p = \frac{3}{4}\frac{\eta \dot{h}}{h^3}\left(R^2 - r^2\right)$. Integrating over area of the disk, the force the fluid exerts on the disk (Eqn. (4)) becomes $F_N = \frac{3\pi}{8}\frac{\eta \dot{h}}{h^3}R^4$. To find the relationship between force and radius or area of disk, we simplify with defining a constant $C \equiv \frac{3\pi}{8}\frac{\eta \dot{h}}{h^3}$ which gives $F_N = CR^4$. The total area A for n surface features of radius R_n is $A = n\pi R_n^2$, where the subscript n denotes multiple surface features. Comparing the force of the un-patterned pad with a single feature to that with n features, $F_{N,\,tot} = nF_{N,\,n} = nCR_n^4 = nC\frac{R_1^4}{n^2} = \frac{1}{n}R_1^4$. The total normal force scales with the inverse of feature number, hence Eqn. (5).

REFERENCES

[1] F. Negrello, H. S. Stuart, and M. G. Catalano, "Hands in the real world," *Frontiers in Robotics and AI*, vol. 6, p. 147, 2020.

[2] "Tokyo Univ. Technology that supports dish washing with kitchen robots," 2008. [Online]. Available: http://www.irt.i.u-tokyo.ac.jp/en/reform/081217/index.shtml

[3] E. Ackerman, "Dishcraft Robotics Takes Over Dishwashing From Humans - IEEE Spectrum," June 2011. [Online]. Available: https://spectrum.ieee.org/automaton/robotics/industrial-robots/dishcraft-robotics-takes-over-dishwashing-from-humans

[4] M. Cutkosky, J. Jourdain, and P. Wright, "Skin materials for robotic fingers," in *1987 IEEE International Conference on Robotics and Automation Proceedings*, vol. 4, Mar. 1987, pp. 1649–1654.

[5] E. V. Eason, E. W. Hawkes, M. Windheim, D. L. Christensen, T. Libby, and M. R. Cutkosky, "Stress distribution and contact area measurements of a gecko toe using a high-resolution tactile sensor," *Bioinspiration & biomimetics*, vol. 10, no. 1, p. 016013, 2015.

[6] A. M. Okamura, N. Smaby, and M. R. Cutkosky, "An overview of dexterous manipulation," in *Proceedings 2000 ICRA. Millennium Conference. IEEE International Conference on Robotics and Automation. Symposia Proceedings (Cat. No. 00CH37065)*, vol. 1. IEEE, 2000, pp. 255–262.

[7] Y. Fujihira, K. Harada, T. Tsuji, and T. Watanabe, "Experimental investigation of effect of fingertip stiffness on resistible force in grasping," in *2015 IEEE International Conference on Robotics and Automation (ICRA)*, 2015, pp. 4334–4340.

[8] V. A. Ho and S. Hirai, "Modeling and Analysis of a Frictional Sliding Soft Fingertip, and Experimental Validations," *Advanced Robotics*, vol. 25, no. 3-4, pp. 291–311, Jan. 2011.

[9] M. Guo, D. V. Gealy, J. Liang, J. Mahler, A. Goncalves, S. McKinley, J. A. Ojea, and K. Goldberg, "Design of parallel-jaw gripper tip surfaces for robust grasping," in *2017 IEEE International Conference on Robotics and Automation (ICRA)*, 2017, pp. 2831–2838.

[10] H. X. Trinh, V. A. Ho, and K. Shibuya, "Theoretical Foundation for Design of Friction-Tunable Soft Finger With Wrinkle's Morphology," *IEEE Robotics and Automation Letters*, vol. 4, no. 4, pp. 4027–4034, Oct. 2019.

[11] S. Nojiri, K. Mizushima, Y. Suzuki, T. Tsuji, and T. Watanabe, "Development of Contact Area Variable Surface for Manipulation Requiring Sliding," in *2019 2nd IEEE International Conference on Soft Robotics (RoboSoft)*, Apr. 2019, pp. 131–136.

[12] K. Mizushima, Y. Suzuki, T. Tsuji, and T. Watanabe, "Deformable fingertip with a friction reduction system based on lubricating effect for smooth operation under both dry and wet conditions," *Advanced Robotics*, vol. 33, no. 10, pp. 508–519, 2019.

[13] M. Changizi, R. Weber, R. Kotecha, and J. Palazzo, "Are Wet-Induced Wrinkled Fingers Primate Rain Treads?" *Brain, Behavior and Evolution*, vol. 77, no. 4, pp. 286–290, 2011.

[14] J. Haseleu, D. Omerbašić, H. Frenzel, M. Gross, and G. R. Lewin, "Water-Induced Finger Wrinkles Do Not Affect Touch Acuity or Dexterity in Handling Wet Objects," *PLoS ONE*, vol. 9, no. 1, Jan. 2014.

[15] K. Kareklas, D. Nettle, and T. V. Smulders, "Water-induced finger wrinkles improve handling of wet objects," *Biology Letters*, vol. 9, no. 2, Apr. 2013.

[16] S. P. Landers, B. J. J. Ratliff, C. D. Miller, and J. K. Clark, "Pneumatic Tire Having Improved Wet Traction," 2002.

[17] T. Yamaguchi and K. Hokkirigawa, "Development of a High Slip-resistant Footwear Outsole Using a Hybrid Rubber Surface Pattern," *Industrial Health*, vol. 52, no. 5, pp. 414–423, 2014.

[18] K. Mizushima, T. Nishimura, Y. Suzuki, T. Tsuji, and T. Watanabe, "Surface Texture of Deformable Robotic Fingertips for a Stable Grasp Under Both Dry and Wet Conditions," *IEEE Robotics and Automation Letters*, vol. 2, no. 4, pp. 2048–2055, Oct. 2017.

[19] P. V. Nguyen and V. A. Ho, "Grasping Interface With Wet Adhesion and Patterned Morphology: Case of Thin Shell," *IEEE Robotics and Automation Letters*, vol. 4, no. 2, pp. 792–799, 2019.

[20] B. N. J. Persson, "Wet adhesion with application to tree frog adhesive toe pads and tires," *Journal of Physics: Condensed Matter*, vol. 19, no. 37, p. 376110, Aug. 2007.

[21] C. Menon, M. Murphy, and M. Sitti, "Gecko Inspired Surface Climbing Robots," in *2004 IEEE International Conference on Robotics and Biomimetics, Shenyang*, June 2004, pp. 431–436.

[22] J.-P. Roberge, W. Ruotolo, V. Duchaine, and M. Cutkosky, "Improving industrial grippers with adhesion-controlled friction," *IEEE Robotics and Automation Letters*, vol. 3, no. 2, pp. 1041–1048, 2018.

[23] H. Lee, B. P. Lee, and P. B. Messersmith, "A reversible wet/dry adhesive inspired by mussels and geckos," *Nature*, vol. 448, no. 7151, pp. 338–341, 2007.

[24] S. Wang, H. Jiang, T. Myung Huh, D. Sun, W. Ruotolo, M. Miller, W. R. Roderick, H. S. Stuart, and M. R. Cutkosky, "Spinyhand: Contact load sharing for a human-scale climbing robot," *Journal of Mechanisms and Robotics*, vol. 11, no. 3, 2019.

[25] S. B. Backus, R. Onishi, A. Bocklund, A. Berg, E. D. Contreras, and A. Parness, "Design and testing of the JPL-Nautilus Gripper for deep-ocean geological sampling," *Journal of Field Robotics*.

[26] M. S. Li, R. van der Zande, A. Hernández-Agreda, P. Bongaerts, and H. S. Stuart, "Gripper Design with Rotation-Constrained Teeth for Mobile Manipulation of Hard, Plating Corals with Human-Portable ROVs," in *OCEANS - Marseille*, June 2019, pp. 1–6.

[27] H. Stuart, S. Wang, and M. R. Cutkosky, "Tunable contact conditions and grasp hydrodynamics using gentle fingertip suction," *IEEE Transactions on Robotics*, 2018.

[28] Y. Wang, X. Yang, Y. Chen, D. K. Wainwright, C. P. Kenaley, Z. Gong, Z. Liu, H. Liu, J. Guan, T. Wang, J. C. Weaver, R. J. Wood, and L. Wen, "A biorobotic adhesive disc for underwater hitchhiking inspired by the remora suckerfish," *Science Robotics*, vol. 2, no. 10, 2017.

[29] K. L. Johnson, *Contact Mechanics*. Cambridge University Press, 1985.

[30] B. N. J. Persson, "Theory of rubber friction and contact mechanics," *The Journal of Chemical Physics*, vol. 115, no. 8, pp. 3840–3861, 2001.

[31] N. Xydas and I. Kao, "Modeling of Contact Mechanics and Friction Limit Surfaces for Soft Fingers in Robotics, with Experimental Results," *The International Journal of Robotics Research*, vol. 18, no. 9, pp. 941–950, Sept. 1999.

[32] T. Watanabe and Y. Fujihira, "Experimental investigation of effect of fingertip stiffness on friction while grasping an object," in *2014 IEEE International Conference on Robotics and Automation (ICRA)*, May 2014, pp. 889–894.

[33] P. J. Leider and R. B. Bird, "Squeezing Flow between Parallel Disks. I. Theoretical Analysis," *Industrial & Engineering Chemistry Fundamentals*, vol. 13, no. 4, pp. 336–341, Nov. 1974.

[34] L. M. Diamante and T. Lan, "Absolute Viscosities of Vegetable Oils at Different Temperatures and Shear Rate Range of 64.5 to 4835 s1," 2014.

[35] B. J. Hamrock, S. R. Schmid, and B. O. Johnson, *Fundamentals of Fluid Film Lubrication*. New York, New York: Marcel Dekker, Inc., 2004.

[36] J. S. Sharp, S. F. Poole, and B. W. Kleiman, "Optical Measurement of Contact Forces Using Frustrated Total Internal Reflection," *Physical Review Applied*, vol. 10, no. 3, p. 034051, Sept. 2018.

[37] M. Barquins, "Sliding friction of rubber and Schallamach waves — A review," *Materials Science and Engineering*, vol. 73, pp. 45–63, 1985.